Interrogation of SLFN11 in pediatric sarcomas uncovers an unexpected biological role and a novel therapeutic approach to overcoming resistance to replicative stress

Jessica Gartrell[1], Marcia Mellado-Largarde[2], Nancy E. Martinez[2], Michael R. Clay[3], Armita Bahrami[4], Natasha Sahr[5], April Sykes[5], Kaley Blankenship[1], Lauren Hoffmann[1], Jia Xie[2], Hyekyung Plumley[2], Nathaniel Twarog[2]; Michele Connelly[2]; Koon-Kiu Yan[6], Jiyang Yu[6], Shaina N. Porter[7], Shondra M. Pruett-Miller[7], Geoffrey Neale[8], Christopher L. Tinkle[9], Sara M. Federico[1], Elizabeth A. Stewart[1,10], Anang A. Shelat[2]

[1]Department of Oncology, St. Jude Children's Research Hospital, Memphis, Tennessee. [2] Department of Chemical Biology and Therapeutics, St. Jude Children's Research Hospital, Memphis, Tennessee. [3]Department of Pathology, University of Colorado Anschutz Medical Campus, Aurora, Colorado. [4]Department of Pathology, St. Jude Children's Research Hospital, Memphis, Tennessee. [5]Department of Biostatistics, St. Jude Children's Research Hospital, Memphis, Tennessee. [6]Department of Computational Biology, St. Jude Children's Research Hospital, Memphis, Tennessee. [7]Department of Cell and Molecular Biology and The Center for Advanced Genomic Engineering, St. Jude Children's Research Hospital, Memphis, Tennessee. [8]Hartwell Center for Bioinformatics and Biotechnology, St. Jude Children's Research Hospital, Memphis, Tennessee. [9]Department of Radiation Oncology, St. Jude Children's Research Hospital, Memphis, Tennessee. [10]Department of Developmental Neurobiology, St. Jude Children's Research Hospital, Memphis, Tennessee.

Running Title: The role of SLFN11 in pediatric sarcomas

Keywords: SLFN11, pediatrics, sarcoma, replicative stress

Financial support: This work was supported, in part, by the American Lebanese Syrian Associated Charities (E.A.S., A.A.S.). E.A.S. was supported by the National Comprehensive Cancer Network and is a St. Baldrick's Scholar with generous support from the Invictus Fund. A.A.S. was supported by research grants from the Sarcoma Foundation of America and the St. Baldrick's Foundation.

Corresponding authors: (1) Dr. Elizabeth A. Stewart, Department of Oncology and Department of Developmental Neurobiology, St. Jude Children's Research Hospital, 262 Danny Thomas Place, Memphis, TN 38105. Tel: +1 901-595-3544; Fax: +1 901-521-9005; Email: elizabeth.stewart@stjude.org. (2) Dr. Anang A. Shelat, Department of Chemical Biology and Therapeutics, St. Jude Children's Research Hospital, 262 Danny Thomas Place, Memphis, TN 38105. Tel: +1 901-595-5751; Fax: +1 901-595-5715; Email: anang.shelat@stjude.org.

The authors declare there are no conflicts of interest.

Word count = 5928; Total figures and tables = 7

Abstract

Pediatric sarcomas represent a heterogeneous group of malignancies that exhibit variable response to DNA damaging chemotherapy. Schlafen family member 11 protein (SLFN11) increases sensitivity to replicative stress, and *SLFN11* gene silencing has been implicated as a common mechanism of drug resistance in tumors in adults. We found SLFN11 to be widely expressed in our cohort of pediatric sarcomas. In sarcoma cell lines, protein expression strongly correlated with response to the PARP inhibitor talazoparib (TAL) and the topoisomerase I inhibitor irinotecan (IRN), with SLFN11 knockout resulting in significant loss of sensitivity *in vitro* and *in vivo.* However, SLFN11 expression was not associated with favorable outcomes in a retrospective analysis of our patient cohort; instead, the protein was retained and promoted tumor growth and evasion. Furthermore, we show that pediatric sarcomas develop resistance to TAL and IRN through impaired intrinsic apoptosis, and that resistance can be reversed by selective inhibition of BCL-XL.

Statement of Significance

The role of SLFN11 in pediatric sarcomas has not been thoroughly explored. In contrast to its activity in adult tumors, SLFN11 did not predict favorable outcomes in pediatric patients, was not silenced, and promoted tumor growth. Resistance to replicative stress in SLFN11-expressing sarcomas was reversed by selective inhibition of BCL-XL.

INTRODUCTION

Pediatric sarcomas are a heterogeneous group of malignancies disproportionately affecting adolescents and young adults. Multimodal therapy with chemotherapy, surgery, and radiation therapy (RT) has improved outcomes for those patients with localized disease. However, progress has stalled for patients with metastatic disease, who continue to have survival rates of <30% for the most common subtypes [1-5]. Therefore, novel therapeutic strategies and biomarkers that predict sensitivity to therapy are needed.

Previously, we reported that combining the poly (ADP-ribose) polymerase inhibitor (PARPi) talazoparib (TAL) with the topoisomerase I inhibitor (Topo1i) irinotecan (IRN) and temozolomide (TMZ) resulted in high rates of complete response (CR) in a murine model of Ewing sarcoma (ES) [6]. This work motivated a clinical trial testing TAL plus IRN with and without TMZ in children with refractory/recurrent solid tumors (NCT02392793). Results were encouraging: of 24 evaluable patients, 1 with Ewing sarcoma (ES) had a complete response (CR), 5 others had a partial response (PR), and 18 had disease stabilization [7]. However, it remains unclear how the combination works in this population.

Although BRCA mutations are rare in ES, several mechanisms have been proposed to explain the PARPi sensitivity in ES, most notably *functional* BRCA deficiency and SLFN11 [8-11]. Fusion proteins involving the peptide encoded by *EWSR1* at the N-terminus are the oncogenic drivers in ES (which has *EWSR1-FLI1/ERG* fusion*)* and in a subset of aggressive sarcomas, such as

76 desmoplastic small round cell tumors (DSRCTs) (which have *EWSR1-WT1* fusion) and clear cell
77 sarcomas (which have *EWSR1-ATF1* fusion). Gorthi et al [11] reported that the *EWSR1* fusion
78 protein increases R-Loop formation, which sequesters BRCA1, rendering the tumor cell BRCA
79 deficient and susceptible to replicative stress. They speculated that BRCA deficiency might create
80 a liability in all tumors possessing an *EWSR1*-translocation. Tumors deficient in mediators of
81 homologous recombination (HR) such as *BRCA1* and *BRCA2* are more susceptible to DNA single
82 strand breaks: consequently, PARPis are selectively lethal in these cells. However, in contrast to
83 PARPi treatment of adult tumors with *BRCA1* or *BRCA2* mutations, single-agent PARPi treatment
84 in patients with relapsed/refractory ES elicited no significant responses or durable disease control
85 [12].

86

87 Ewing sarcomas express high levels of Schlafen family member 11 (SLFN11), a putative DNA/RNA
88 helicase whose expression has been associated with the response to DNA damaging agents
89 (DDAs), thymocyte maturation, viral immunity, and interferon production [13]. SLFN11 augments
90 sensitivity to replicative stress by stalling replication forks and impairing the DNA repair
91 checkpoint response [14, 15]. PARPis cause replicative stress through PARP trapping [9], whereby
92 the PARP protein becomes physically associated with DNA. This is similar to the mechanism of
93 action of Topo1is, which are well-known inducers of replicative stress [16]. Additionally, PARP
94 inhibition augments Topo1i toxicity by preventing the recruitment of repair enzymes to the site
95 of damage, and TMZ enhances PARPi-mediated replicative stress by augmenting PARP trapping
96 [17]. Therefore, the strategy of combining a PARPi, a Topo1i, and TMZ is a rational means of
97 exploiting replicative stress in cancer cells. In retrospective studies, patients with ovarian cancer

[18], breast cancer [19], prostate cancer [20], and ES-family tumors [10] who were treated with DDAs had better prognosis if their tumors had high SLFN11 expression. Patients with small-cell lung cancer expressing SLFN11 showed improved progression-free survival (PFS) and overall survival (OS) when treated with the PARPi veliparib and TMZ [21].

Determining whether *SLFN11* or the *EWSR1* fusion drives sensitivity to PARPi combinations in pediatric sarcomas is crucial for identifying patients who might benefit the most from such treatment. Although SLFN11 is highly expressed in ES, its expression pattern in other pediatric sarcomas is largely unknown. *SLFN11* mutations are rare, and epigenetic regulation has been suggested as a mediator of resistance [16, 22]. In this work, we show that SLFN11 is widely expressed in common pediatric sarcoma subtypes and that the SLFN11 protein, not the presence of a *EWSR1* fusion, drives sensitivity to TAL and IRN both *in vitro* and *in vivo*. Importantly, we show that SLFN11 expression does not portend a better prognosis in these patients: in fact, we reveal an unexpected oncogenic role for the protein. We also show that impairment of intrinsic apoptosis, not loss of SLFN11 expression, is a primary means of resistance to PARPi combination therapy in pediatric sarcoma, and that sensitivity to TAL+IRN can be restored by selective inhibition of BCL-XL. Our work supports the use of combinations involving strong-trapping PARPis and Topoi1s as targeted therapy for SLFN11-positive pediatric sarcomas, and it offers novel strategies to combat tumors resistant to replicative stress.

RESULTS

SLFN11 Expression Is Highly Correlated with Sensitivity to SN-38 and TAL

To determine the extent to which SLFN11 expression is correlated with sensitivity to DDA, we analyzed the Genomics of Drug Sensitivity in Cancer (GDSC) database which contains more than 1000 cell lines that have been assayed for cell viability 72 h after exposure to hundreds of drugs [23]. The efficacies of several DDAs, as measured by the area under the curve (AUC), were highly correlated with SLFN11 expression, with those of the strong-trapping PARPi TAL, and SN-38, the active metabolite of IRN, showing the highest statistical significance and the largest effect sizes (**Fig. 1A; Supplementary Table S1A**). In contrast, the microtubule inhibitors vinorelbine and vinblastine and the weak-trapping PARPi olaparib showed poor associations. The Pearson correlation between the mean AUC of SN-38 and TAL was 0.51 ($P < 0.001$), and there was a clear trend between this average and the increasing quintiles of SLFN11 expression ($P < 0.001$, 1-way ANOVA) (**Fig. 1B; Supplementary Table S1B**). We observed no correlation between drug response and those genetic lesions known to impair HR and sensitize tumor cells to both PARPis and Topo1is, such as BRCA1, BRCA2, and ATM (**Fig. 1C; Supplementary Fig. S1A and S1B; Supplementary Table S1C-S1E**) [24-26]. The short timescale of the GDSC viability assay (72 h) suggests that SLFN11 induces rapid cytotoxicity, and this phenotype appears to be distinct from that induced by HR defects.

We further explored the GDSC database by first defining cell lines within the top quintile of expression as “SLFN11 High” and all others as “SLFN11 Low” then examining the distribution of AUCs by tumor subtype (**Fig. 1D**). The correlation between SLFN11 expression and average SN-

38/TAL activity was present in ES, rhabdomyosarcoma (RMS), and osteosarcoma (OST) cell lines, although sampling was low for the latter 2 tumor types. In contrast, all but 1 neuroblastoma model expressed low SLFN11, despite 11/24 cell lines (46%) showing a drug response comparable to that of the highest quintile of SLFN11 expressors. Moreover, there was little difference in the drug response of high and low SLFN11 expressors in glioma cell lines, suggesting that the potential for SLFN11 to act as a biomarker predicting sensitivity to SN-38/TAL varies considerably across tumor types.

To better understand the relation between SLFN11 levels and DNA repair defects, we calculated mutational signatures (MS) in tumors from pediatric patients with ES, RMS, and OST (**Fig. 1E and 1F; Supplementary Table S1F**), using data from BRCA-deficient and BRCA-wild-type cohorts used as control [27]. As expected, expression of MS3, a signature associated with HR repair defects, was highest in the BRCA-deficient group. Consistent with recent reports, OST also showed elevated expression of this signature [28]. In contrast, ES tumors had MS3 levels comparable to those in BRCA-wild-type tumors, a finding inconsistent with reports that suggest translocations involving *EWSR1* induce functional BRCA deficiency. Consistent with previously reported whole-genome sequencing studies [29, 30], ES tumors have low genomic instability as assessed by the total number of mutations—an observation incompatible with the presence of HR deficiency.

Given the high level of SLFN11 expression in ES and the relative scarcity of data on its expression in other pediatric sarcoma, we developed an immunohistochemistry (IHC) protocol that uses a

commercially available antibody to assess protein levels in pediatric sarcomas directly. We assayed 353 samples from 220 different patients with non-CNS solid tumors who had sufficient material for staining at St. Jude Children's Research Hospital (**Fig. 1G; Supplementary Table S1G and S1H).** The patient demographics and diagnosis groups are shown in **Table 1**. SLFN11 had variable expression, but was nearly universal in ES and DSRCT, with 90% and 100% of those tumors showing SLFN11 positivity (H-score > 0), respectively. SLFN11 was detected in 75% of the samples from patients with OST or embryonal RMS (eRMS). Quantification of SLFN11 in the other tumor types was limited by the small sample sizes. Using H-score at diagnosis, we found the highest SLFN11 expression in ES, followed by eRMS, OST, and DSRCT **(Fig. 1H**), with a few samples of the latter 3 tumor types having high expression levels similar to those observed in ES. Overall, SLFN11 was expressed in 69% of pediatric sarcoma sampled, and 76% of the most common pediatric sarcomas—a significantly higher percentage than has been implicated in adult tumors [31].

SLFN11, Not *EWSR1* Translocation, Is Required for Sensitivity to SN-38 and TAL *In vitro*

To further assess SLFN11 and *EWSR1* translocation as potential drivers of sensitivity to TAL and SN-38, we profiled 14 sarcoma cell lines that varied by translocation type, p53 status, and histology, then we assessed SLFN11 expression by IHC, Western blot, and qPCR analysis (**Fig. 2A, Supplementary Table S2A and S2B**). The Pearson correlation between SLFN11 protein and mRNA levels was 0.64 (P = 0.018) (**Supplementary Fig. S2A**). Protein levels were correlated with sensitivity to single-agent SN-38 and TAL, with Pearson correlations of 0.72 (P = 0.003) and 0.74

183 ($P = 0.003$), respectively (**Supplementary Fig. S2B**); and with the mean AUC of the 2 compounds,
184 with a Pearson correlation of 0.77 ($P = 0.001$) (**Fig. 2B)**. We found no association between
185 sensitivity to these drugs and p53 status ($P = 0.12$, *t-test*) (**Supplementary Fig. S2C**). Although
186 most *EWSR1*-translocated cell lines were more sensitive to drug treatment when compared to
187 non-translocated cell lines, they also tended to express the highest levels of SLFN11. The
188 exception was SU-CCS-1, a SLFN11-negative (no protein detected by Western; IHC H-score = 0)
189 *EWSR1-ATF1*-translocated clear cell sarcoma, suggesting that the *EWSR1* translocation alone was
190 insufficient to drive drug sensitivity.

191

192 To confirm SLFN11 as the primary driver of sensitivity to these agents, we knocked out the gene
193 by using CRISPR/Cas9 in our 3 highest-expressing models, generating the isogenic pairs: ES8/ES8-
194 KO, JN-DSRCT/JN-DSRCT-KO, and A673/A673-KO. We also over-expressed the protein in U2OS
195 cells, which showed little baseline expression, to create U2OS-OE cells (61% protein relative to
196 total ES8 by Western); and in ES8-KO cells, to create ES8-KO+OE cells (37% protein relative to
197 total ES8). Knockout and over-expression were confirmed by Western blot analysis and IHC
198 (**Supplementary Figure S2D and S2E; Supplementary Table S2A and S2B**). Loss of SLFN11 protein
199 significantly reduced sensitivity to both SN-38 and TAL in all three knockout lines, whereas over-
200 expression in U2OS and ES8-KO cells increased drug sensitivity (**Fig. 2C and 2D**). Consistent with
201 our GDSC analysis, SLFN11 loss had little effect on vincristine sensitivity. Despite expressing a
202 lower level of the same engineered SLFN11 protein construct, ES ES8-KO+OE cells had higher AUC
203 values for SN-38 and TAL when compared to OST U2OS-OE cells (0.40 vs. 0.25 for SN-38 and 0.26
204 vs. 0.10 for TAL), consistent with the hypothesis that the magnitude of sensitization induced by

SLFN11 varies between tumor types (**Supplementary Fig. S2F**). Ionizing radiation is another means to induce replicative stress [32]. In agreement with our SN-38 and TAL experiments, ES8-KO and JN-DSRCT-KO were more viable, and U2OS-OE was less viable, compared to their wild-type counterparts at 72 h after exposure to 4 Gy radiation (**Supplementary Fig. S2G**).

To further study the effect of SLFN11 KO in our models, we used flow cytometry to compare cell cycle effects and the degree of cell death induced by "Low" (10 nM SN-38 + 10 nM TAL) and "High" (1000 nM SN-38 + 1000 nM TAL) dose combinations after 24 h exposure. Based on our previous pharmacokinetic assessment, "Low" approximates to the upper bound of clinically relevant concentrations for both drugs, whereas "High" is physiologically unobtainable but useful for studying mechanism and resistance [6]. Wild-type ES8 cells showed near-complete loss of viability at both "Low" and "High" doses of the combination, whereas the ability of SN-38+TAL to induce cell death in ES8-KO cells was significantly diminished, even at high concentrations (**Fig. 2E)**. A similar decrease in cell viability was observed in JN-DSRCT compared to JN-DSRCT-KO cells, and the combination was also less cytotoxic in SLFN11-negative SU-CCS-1 cells (**Supplementary Fig. S2H**). SLFN11 selectively induces death in cells arrested in S-phase because of replicative stress [15]. Consistent with this finding, we observed a significant build-up of S-phase-arrested ES8-KO cells (**Fig. 2F**).

Previous studies have shown that SLFN11 is a transcriptional target of EWS-FLI1 [10]. To determine whether SLFN11 itself contributes to the regulation of EWSR1-FLI1 target genes, we

assessed gene expression in ES8 and ES8-KO cells at 4 h and 24 h following exposure to 0 or 2 Gy of ionizing radiation (baseline and stress conditions). EWSR1-FLI known targets mapped equally between upregulated and downregulated genes, and we found no enrichment of directional activation or inhibition of those EWSR1-FLI1 target genes when using Gene Set Enrichment Analysis (GSEA, FDR > 0.05) (**Fig. 2G; Supplementary Table S2C)**. Therefore, although SLFN11 is regulated by EWS-FLI1, it appears to perturb gene expression independently of the fusion protein.

To determine whether SLFN11 influenced the extent of DNA damage induced by SN-38 and TAL, we performed an alkaline comet tail assay after exposing ES8 and ES8-KO cells to DMSO and the "High" concentration of SN-38 and TAL for 2 h (**Fig. 2H**). The amount of DNA damage was similar in both cell lines after drug treatment, indicating that SLFN11 does not enhance the degree of damage but rather increases the probability of cell death following drug insult. Finally, given the findings of high levels of R-loops in *EWSR1*-translocated tumors [11], we quantified R-loop expression in ES8 and ES8-KO cells. Despite a remarkable difference in their response to SN-38 and TAL, we found no significant difference in R-loop levels in the wild-type and SLFN11 KO models (**Fig. 2I)**.

SLFN11, Not *EWSR1* Translocation, Is required for Sensitivity to TAL and IRN *In Vivo*

To confirm our *in vitro* finding indicating that SLFN11 was an important driver of drug response in *EWSR1*-translocated tumors, we conducted *in vivo* efficacy studies, as described previously [6],

using luciferase-labeled xenografts of ES8, ES8-KO, JN-DSRCT, JN-DSRCT-KO, and SU-CCS-1 cells. Mice were screened weekly by Xenogen® imaging and enrolled in the study after a target bioluminescence signal of 10^7 photons/s/cm^2 or a palpable tumor was obtained. We used clinically relevant doses and schedules for all treatment groups tested (**Fig. 3A**) [6] and administered 4 courses of therapy (21 days/course).

In ES8 (high SLFN11) xenografts, mice treated with TAL+IRN+TMZ had the best response, with 100% surviving the 84 days of therapy, and 75% experiencing a CR or PR as determined by the bioluminescence signal (**Fig. 3B and 3C; Supplementary Table S3**). Mice treated with TAL+IRN survived an average of 60.5 days, with 50% surviving all 4 courses of therapy. In sharp contrast to mice with wild-type ES8 xenografts, mice with ES8-KO xenografts treated with TAL+IRN and TAL+IRN+TMZ survived an average of 7.5 days and 23.1 days, respectively, with 100% having progressive disease (PD) (**Fig. 3D and 3E; Supplementary Table S3**). No mice in any ES8-KO treatment cohort survived all 4 courses of therapy, although 1 control mouse appeared to have lost its engraftment signal after 2 weeks and survived the study. Compared to ES8 mice, survival in ES8-KO mice was significantly lower when treated with either TAL+IRN ($P < 0.001$) or TAL+IRN+TMZ ($P < 0.001$) (**Fig. 3F**).

Testing JN-DSRCT (high SLFN11) xenografts *in vivo* was challenging, as these tumors grew slower and had lower engraftment rates by comparison with ES8 xenografts. Five wild-type mice were successfully enrolled and treated with either TAL+IRN or TAL+IRN+TMZ, and all experienced a CR

by 84 days (**Fig. 3G and 3H; Supplementary Table S3**). One untreated mouse was also enrolled and maintained stable disease (SD) throughout the 4 courses of therapy. Interestingly, JN-DSRCT-KO cells engrafted poorly and were unable to be tested. In SU-CCS-1 (no SLFN11) xenografts, disease stabilized in mice treated with TAL+IRN+TMZ and 90% of the mice had SD or a PR at the end of therapy (**Fig. 3I**). However, once therapy was stopped, all mice regrew tumors within a few weeks (**Fig. 3J**). Together, these findings confirm the importance of SLFN11 in driving *in vivo* sensitivity to combinations involving SN-38 and TAL in *EWSR1*-translocated tumors. The most striking result was the near complete loss of efficacy in ES8-KO xenografts.

Finally, we explored efficacy in 143B cells, an aggressive OST cell line (*EWSR1* fusion negative) with low SLFN11 expression (19% of that in ES8 cells), and observed an intermediate response. Mice treated with TAL+IRN survived an average of 13.4 days, with 100% having PD (**Supplementary Fig. S3; Supplementary Table S3**). However, mice treated with TAL+IRN+TMZ survived much longer, with an average of 77.8 days on study, although none experienced a CR.

SLFN11 Positivity Is Not Associated With Better Outcomes in Children With Sarcoma

Motivated by the strong evidence that SLFN11 sensitized pediatric sarcomas to PARPi combination therapy *in vitro* and *in vivo*, we performed a retrospective analysis of the patient cohort profiled in our IHC study to determine how SLFN11 status changed as therapy progressed and whether protein levels predicted clinical outcome. Only patients who had a sample available prior to recurrence or progression were included in the survival analysis (N = 143, **Table 1**). 98.4%

289 of patients were treated with at least one DDA and 66.7% received radiation at some point in
290 their therapy. This population was more refractory than would be expected historically, with
291 patients with NRSTS, ES, and eRMS all having OS and event-free survival (EFS) of <50% at 5 years
292 (**Fig. 4A; Supplementary Fig. S4A).**

293

294 Loss of SLFN11 expression has been proposed as a mechanism of DDA resistance in adult tumors
295 [33]. To explore the trend of SLFN11 levels in our cohort, we identified 18 patients with at least
296 2 IHC measurements spanning different points in treatment (**Fig. 4B; Supplementary Fig. S4B**).
297 We found no evidence that SLFN11 was silenced over time: 10/18 of patients remained positive
298 throughout, 3/18 went from being SLFN11 negative to SLFN11 positive, 3/18 went from being
299 SLFN11 positive to SLFN11 negative, and 2/18 were initially SLFN11 positive then had a negative
300 sample followed by another positive sample. When including all patients in our IHC study, 37.2%
301 of those with a sample at diagnosis were positive, compared with 46.2% at progression and 53.7%
302 at relapse (**Supplementary Table S4A**). We observed no clear trend in the mean values for SLFN11
303 H-score in samples obtained at diagnosis, relapse, or autopsy.

304

305 Using receiver-operating characteristic (ROC) analysis, we found that SLFN11 expression as
306 measured by H-score failed to discriminate patients by EFS, OS, recurrence-free survival (RFS), or
307 PFS across all tumor types (**Fig. 4C; Supplementary Fig. S4C-S4E**), or within individual disease
308 cohorts (**Fig. 4D; Supplementary Fig. S4F and S4G**). Surprisingly, SLFN11 positivity was a
309 statistically significant predictor of *worse* outcome in terms of RFS ($P = 0.045$, HR = 1.76 [1.01-

3.05]) in univariate analysis (**Supplementary Table S4B**). The metrics OS ($P = 0.072$, HR = 1.82 [0.95-3.49]), EFS ($P = 0.10$, HR = 1.58 [0.92-2.73]), and PFS ($P = 0.078$, HR = 1.72 [0.94-3.13]) were nonsignificantly associated with poorer outcomes in patients with SLFN11 expressing tumors. Although statistical significance was not achieved for any metric in multivariate analysis controlling for age, metastatic status, and disease, the hazard ratio for positivity remained at or greater than unity (**Fig. 4E; Supplementary Fig. S4H-S4J).** ROC analysis using the H-scores failed to discriminate patients with metastatic disease (AUC = 0.605). Moreover, neither SLFN11 H-score nor positivity were statistically significant predictors of metastasis in multivariate analysis that controlled for diagnosis ($P = 0.58$ and 0.35, respectively).

To further interrogate the impact of SLFN11 expression in pediatric sarcoma, we developed and characterized an orthotopic xenograft model, SJEWS049193_X1, using a tumor obtained at autopsy from a patient with metastatic ES treated with multiple salvage regimens, including treatment on the TAL+IRN+TMZ clinical trial NCT02392793 (**Fig. 4F)**. Despite expressing a high level of SLFN11 (H-score = 285), this tumor failed to respond to TAL+IRN+TMZ *in vivo*, and 100% of mice showed PD (**Fig. 4G-4I, Supplementary Table S3**). Taken together, our clinical findings indicated that (a) SLFN11 positivity is common in pediatric sarcoma; (b) pediatric sarcomas do not acquire DDA resistance via *SLFN11* silencing; and (c) SLFN11 positivity does not predict improved patient outcomes, and might, in fact, do the opposite. These results suggest an oncogenic role for SLFN11 in these tumors.

SLFN11 Knockout Induces Widespread Transcriptional Changes in Models of ES and DSRCT

To investigate the effect of SLFN11 beyond its role as a sensitizer to DNA damage, we expanded the microarray study described earlier to include JN-DSRCT and JN-DSRCT-KO cells (**Fig. 5A**). After controlling for cell of origin, 4960/21148 of the genes studied (23%) were differentially expressed in ES8 and JN-DSRCT upon SLFN11 loss (ANOVA FDR < 0.05). GSEA using the MsigDB Hallmark sets [34] revealed significant upregulation of genes involved in "Interferon Alpha Response", "Interferon Gamma Response", and "TNFA Signaling via NFKB"; and downregulation of genes enriched in "E2F targets" and "G2M Checkpoint" (FDR q-value < 0.001, **Fig. 5B; Supplementary Fig. S5A**) in SLFN11-KO cells. Ingenuity Pathway Analysis (IPA) [35], based on differentially expressed genes showing concordant change greater than 0.2 log in both cell backgrounds, confirmed "Interferon Signaling" activation in SLFN11-KO cells. The top regulator effect identified by IPA was enhanced "Quantity of MHC Class I on cell surface" in SLFN11-KO cells (**Fig. 5C**). This expression study suggests that loss of SLFN11 decreases proliferation and reduces evasion of the host innate immune response in these models.

The most upregulated gene in SLFN11-KO cells was that encoding arginase succinate synthetase 1 (ASS1), an enzyme involved in the arginine biosynthetic pathway (**Fig. 5D**). Others have shown that tumor cells repress the *ASS1* gene to bypass the urea cycle and increase cytosolic aspartate levels, thereby stimulating pyrimidine biosynthesis and promoting cancer proliferation [36, 37]. ASS1 deficiency is common in sarcomas, and renders them vulnerable to depletion of arginine from their environment via pegylated arginine deiminase (ADI-PEG 20) [38, 39]. To test whether changes in *ASS1* expression had functional consequences, we treated ES8 and JN-DSRCT wild-type and SLFN11-KO cells with ADI-PEG 20 in a dose-response experiment and then evaluated

354 cell viability with the CellTiter-Glo (CTG) assay. Consistent with our expression study, wild-type
355 cells were more sensitive to arginine depletion than were SLFN11-KO cells (**Fig. 5E**).

356

357 To determine whether the presence of SLFN11 conferred a general growth advantage to sarcoma
358 cells, we measured the growth rate of wild-type and SLFN11-KO cells in culture. We observed
359 decreases of 9%, 17%, and 27% in the growth rates for KO cells compared to wild-type ES8, JN-
360 DSRCT, and A673 cells, respectively; and an increase of 7% for U2OS-OE cells compared with
361 U2OS cells (**Figure 5F; Supplementary Fig. S5B**). *In vivo*, ES8 and ES8-KO models maintained the
362 aggressive growth observed *in vitro* and we were unable to detect a difference in survival
363 between untreated mice from these two groups ($P = 0.316$) (**Supplementary Table S3**). Strikingly,
364 SLFN11 deletion caused a complete loss of the ability of JN-DSCRT-KO cells to form tumors in our
365 xenograft models, despite multiple attempts to optimize conditions both intraperitoneally and
366 subcutaneously (**Fig. 5G)**.

367

368 **Mechanisms of Resistance to SN-38 and TAL in SLFN11-Expressing Pediatric Sarcomas**

369 The lack of SLFN11 silencing in the pediatric sarcoma population led us to seek alternative
370 mechanisms of resistance in cell lines with high levels of SLFN11 expression. Unfortunately,
371 SJEWS049193_X1, the resistant ES model described earlier, was not amenable to prolonged cell
372 culture and *in vitro* investigation. Therefore, we mined the GDSC database to identify the
373 sarcoma cell lines with the highest levels of SLFN11 expression that were refractory (having less
374 than the median activity observed in the GDSC) to both SN-38 and TAL. We identified 3 lines of

interest: EW-13, EW-18, and EW-24 (**Supplementary Fig. S6A**, bottom-left quadrant). These lines showed broad resistance to oncology drugs, including vincristine, when compared to sensitive ES models with high SLFN11 expression (**Fig. 6A; Supplementary Table S6A)**. We obtained EW-13 and EW-18, as well as EW-11 which showed intermediate sensitivity in the database. Separately, we acquired CHLA258, which was reported to be less sensitive to Topo1is [40]. We confirmed drug resistance with CTG assays and flow cytometry (**Fig. 6B; Supplementary Fig. S6B**). Western blot analysis indicated strong SLFN11 expression, with bands of appropriate size, in EW-11, EW-13, and CHLA258; however, protein expression in EW-18 was weaker and the band migration corresponded to a lower molecular weight (**Fig. 6C; Supplementary Fig. S6C**). Cross-referencing with the COSMIC database (https://cancer.sanger.ac.uk/cosmic) revealed that the *SLFN11* gene in EW-18 had a frameshift mutation, c.1928_1929insA, which resulted in a C-terminal truncation that was predicted to limit nuclear localization and, therefore, reduce DDA sensitization [14]. Indeed, IHC confirmed that SLFN11 was predominantly expressed in the cytoplasm, and consequently, the cell line was assigned an H-score of 0 (**Fig. 6D; Supplementary Fig. S6D**). It is important to note that, as far we are aware, all commercially available antibodies target the N-terminus of SLFN11 and could fail to detect C-terminal truncations unless a distinction is made between nuclear and cytoplasmic staining as we did in this study.

Although the *SLFN11* mutation in EW-18 could explain its weak response to DDAs, our analysis of the GDSC and COSMIC databases indicated that the frequency of *SLFN11* mutation in the resistant population was low, with 18/22 cell lines (82%) having a wild-type sequence. We chose SLFN11-wild-type CHLA258 for further investigation. We confirmed strong nuclear expression of

the protein by IHC (H-score = 225) (**Fig. 6D**). Consistent with the other tumor lines, SN-38+TAL induced a high level of DNA damage as assessed by the alkaline comet-tail assay (**Fig. 6E**). R-loop expression was comparable to that observed in ES8 and ES8-KO cells (**Fig. 6F**). The "Low" combination of SN-38 and TAL did not substantially increase apoptosis but instead induced a build-up of S-phase cells similar to that observed with ES8-KO cells (**Supplementary Fig. 6SE)**. However, the S-phase population was depleted by the "High" concentration.

Overlaying the SN-38 dose-response curves for the ES8, ES8-KO and resistant cell lines revealed 2 distinct phenotypes (**Fig. 6G**). The dose-response curves for EW-11, EW-13, CHLA258, and A673 (the least sensitive ES cell line in our original panel) showed an inflection at concentrations of <10 nM, as seen with ES8 cells, but did not show the same level of maximum efficacy (percentage inhibition of viability). Consistent with the lack of SLFN11 nuclear localization, EW-18 behaved more like the ES8-KO cells. The efficacy of TAL was substantially less in all cell lines, and its potency was 2 to 6-fold within that in ES8 cells. The exceptions to this were EW-13, in which TAL was more potent than in ES8 cells, and EW-18, in which TAL was inactive (**Supplementary Fig. S6F**).

To probe the mechanism of cytotoxicity induced by TAL and SN-38, we treated ES8 cells exposed to each drug with the caspase inhibitor Z-VAD-FMK, and discovered a significant reduction in efficacy suggesting that apoptosis was the primary mode of cell death with this drug combination (data not shown). To investigate the role of the intrinsic apoptosis pathway in mediating drug

418 sensitivity, we knocked out BAX, BAK, and both BAX and BAK in ES8 cells. The potency of SN-38
419 and TAL in BAX and BAX/BAK KO cells remained within 2-fold of that in wild-type ES8 cells, but
420 their efficacy was significantly reduced—a phenotype similar to that observed in EW-11, EW-13,
421 CHLA258, and A673 (**Fig. 6H**). BAX deletion alone reduced sensitivity to the DDAs doxorubicin and
422 etoposide to levels comparable to those in ES8-KO cells, but the deletion also reduced sensitivity
423 to vincristine—a phenotype distinct from that of SLFN11 KO cells and comparable to that
424 observed in the resistant ES cell lines described earlier (**Fig. 6I**).

425

426 During this project, it was reported that resistance to the PARPi olaparib in ES cell lines could be
427 overcome with the pan-BCL2 inhibitor navitoclax [41]. Motivated by that work and by our own
428 findings, we screened small molecules inhibitors that were selective for individual BCL2 family
429 members: venetoclax (BCL2), S63845 (MCL), and A-1331852 (BCL-XL). BCL-XL inhibition alone
430 sensitized sarcoma cells to the combination of SN-38 and TAL (**Fig. 6J**). Addition of A-1331852
431 decreased cell viability in A673 and CHLA-258 by a factor of 5.2- and 7.9, respectively, relative to
432 that with the "Low" concentration alone. Although BCL-XL inhibition enhanced the efficacy of the
433 combination in SLFN11-negative U2OS cells, the change in U2OS-OE cells was significantly greater
434 (a 7.5-fold increase vs. a 2.8-fold increase).

435

436 These mechanistic studies suggest that (a) impairment of the intrinsic apoptotic pathway, rather
437 than reduced SLFN11 expression, constitutes a primary means of resistance to TAL and SN-38 in

pediatric sarcomas; and (b) selective inhibition of BCL-XL can restore sensitivity to the drug combination in SLFN11 expressing resistant tumors.

DISCUSSION

The heterogeneous and aggressive nature of pediatric sarcomas makes it imperative to identify biomarkers for drug response and new therapeutic targets. Preliminary results from the phase I clinical trial NCT02392793 showed that the combination of TAL and IRN was tolerable and yielded encouraging results in several patients with sarcoma. In a phase I/II trial, TAL+TMZ was also well tolerated; however, no tumor response was seen in the 10 patients with ES treated on that trial, although 2 had prolonged SD [42]. Here, we have shown that SLFN11, not *EWSR1*-fusion or functional BRCA deficiency, is a significant driver of sensitivity to TAL and IRN in this population.

Using IHC, we found that SLFN11 was widely expressed in our cohort of patients with pediatric sarcomas, with H-scores reaching near maximum in some samples. The sensitivity to TAL and SN-38 in sarcoma cell lines correlated with protein levels both *in vitro* and *in vivo* and was independent of the *EWSR1* translocation. However, despite the strong link between protein expression and DDA sensitivity in our preclinical studies, we found no association between SLFN11 status and improved outcome in a retrospective analysis of our patient cohort. Moreover, we found no evidence that SLFN11 was silenced in recurrent disease. These findings contradict recent reports indicating that certain SLFN11-positive tumors have better outcomes with DDA therapy and that gene silencing is a principal route to DDA resistance.

459

460 The contrast between our findings and studies in other tumor backgrounds could be attributed
461 to the unique role that SLFN11 plays in pediatric sarcomas. SLFN11 KO in sarcoma cells induced
462 significant changes in transcription, including upregulation of interferon signaling and MHC Class
463 I antigen presentation, and downregulation of genes required for cellular proliferation and
464 oncogenic metabolism. SLFN11-wild-type cells were more sensitive than SLFN11 KO cells to
465 arginine depletion using ADI-PEG-20, confirming the functional consequence of our finding that
466 SLFN11 deletion increased levels of ASS1, the rate-limiting factor in arginine biosynthesis.
467 Moreover, SLFN11 expressing cells grew faster in cell culture, and JN-DSRCT cells engrafted better
468 in orthotopic xenograft models compared to JN-DSCRT-KO cells.

469

470 Importantly, we identified sarcoma models expressing high levels of SLFN11 that were resistant
471 to TAL and SN-38. With the exception of EW-18, in which the *SLFN11* gene was truncated, these
472 tumor cell lines expressed wild-type protein as determined by Western blot analysis, sequence
473 analysis, and nuclear localization. We saw no changes in R-loop levels or in the extent of drug-
474 induced DNA damage. These resistant models compensate for the DDA vulnerability induced by
475 SLFN11 expression by attenuating intrinsic apoptosis. Selective inhibition of BCL-XL increased the
476 cytotoxicity of the combination of TAL and SN-38 in resistant ES cell lines, and resulted in
477 enhanced drug efficacy in OST U2OS cells engineered to over-express SLFN11.

478

Our retrospective analysis of SLFN11 and outcome in pediatric sarcoma was clearly limited. Although most patients received at least 1 DDA, the treatment modalities and disease types varied widely. Moreover, our population appeared to be more refractory to therapy than what would be expected, likely owing to the categories of patients treated at our institution. Consequently, our work strongly supports the prospective evaluation of SLFN11 as a biomarker predicting the response to PARPi and Topo1i combinations in newly diagnosed pediatric sarcomas, which are less likely to have developed widespread chemo-resistance. The ability to rescue tumors by selective BCL-XL inhibition warrants further investigation of strategies that target both replicative stress and the intrinsic apoptotic pathway. Finally, enhanced ASS1 deficiency in SLFN11-positive sarcomas may render them more susceptible to arginine depletion strategies. Ultimately, our work provides a framework to develop rational, targeted combination therapy approaches for both treatment naïve and refractory SLFN11-positive pediatric sarcoma.

METHODS

Genomics of Drug Sensitivity in Cancer (GDSC) Correlations

Drug sensitivity (v17.3) and expression data were downloaded from the GDSC website (https://www.cancerrxgene.org/gdsc1000/GDSC1000_WebResources/Home.html) in May 2018 and June 2018, respectively. COSMIC mutation data (CosmicMutantExport.tsv.gz) was downloaded from https://cancer.sanger.ac.uk/cosmic/download in March 2020.

Mutational Signatures

The set of 30 mutational signatures, a 96 x 30 matrix *Z*, were obtained from COSMIC (https://cancer.sanger.ac.uk/cosmic/signatures). Details of the fitting procedure are provided in Supplemental Data.

Immunohistochemical staining of pediatric tumor samples

Immunohistochemistry was performed with the Dako Omnis instrument (Agilent) on 4-µm-thick formalin-fixed paraffin-embedded whole-tissue sections, using a rabbit anti-SLFN11 (anti-Schlafen family member 11) polyclonal antibody (Sigma-Aldrich Cat# HPA023030, RRID:AB_1856613) (1:25 dilution, 60 min incubation), Dako Low pH Target Retrieval Solution, and the Dako EnVision Flex Detection Kit. Immunoreactivity was scored using H-scores as described in Supplemental Data.

Cell culture and viability assays

Description, sourcing, and culture conditions for the sarcoma cell lines used in this work are reported in **Supplementary Table S2A**. Cell lines were authenticated using short tandem repeat analysis via PowerPlex (Promega), and tested for mycoplasma using MycoAlert (Lonza). Translocation status was confirmed using PCR and Fluorescence In Situ Hybridization (FISH). Cell viability was assessed using the CellTiter-Glo (CTG) assay (Promega). ADI-PED 20 was provided by Polaris Pharmaceuticals (San Diego, CA). Cell line characterization by Western Blot and qPCR analysis is described in Supplemental Data.

520

521 ***Cell Engineering***

522 SLFN11 cDNA (OriGene Technologies Cat# RC226247L4) and the pVector control vector (OriGene
523 Technologies Cat# PS100093) were used to generate the ES8-KO+OE, U2OS-OE, and U2OS-PV
524 models, respectively. hSLFN11$^{-/-}$ cells were generated using CRISPR-Cas9 technology.

525

526 ***Comet Assay***

527 Alkaline single cell electrophoresis was performed using the CometAssay Reagent kit (Trevigen
528 Cat# 4250-050) in accordance with the manufacturer's instructions. Comets were imaged by
529 using the LionHeart FX automated microscope (Biotek) and the Gen5 Image Prime software to
530 construct image montages that were analyzed using TriTek CometScore 2.0.0.38.

531

532 ***R-Loop Immunofluorescence***

533 R-loops were quantified based on the total nuclear intensity of the S9.6 antibody (Kerafast Cat#
534 ENH001, RRID:AB_2687463). Cells were imaged with a Leica microscope using 40x and 63x
535 objectives. Images were acquired using the Photon Counting 3D Nyquist technique.

536

537 ***Expression Analysis by Microarray***

538 Expression profiles were generated from biological triplicates of wild-type and SLFN11-null cells
539 from two parental cell lines (ES8, JNDS). Cells were treated with 0 or 2 Gy of gamma irradiation

then harvested at 4 h or 24 h post-irradiation. Total RNA (100 ng) was purified from treated cells with a RNeasy Mini Kit (Qiagen Cat# 74104) and analyzed using the Affymetrix Clariom S Human assay (ThermoFisher Scientific Cat# 902927).

Patient Correlations

The St. Jude electronic database was surveyed for solid tumor patients enrolled on St. Jude trials from 2000 to 2018 to identify potential samples. Samples were assessed for viability and availability. Once staining was performed, a retrospective review of the electronic medical record was conducted. Patient data were matched with the IHC samples, and the results were analyzed for correlation by an independent statistician.

In Vivo Experiments

Athymic nude immunodeficient mice were purchased from Charles River (strain code 553). This study was carried out in strict accordance with the recommendations in the Guide to Care and Use of Laboratory Animals of the National Institute of Health. The protocol was approved by the Institutional Animal Care and Use Committee at St. Jude Children's Research Hospital. Drug dosing and efficacy studies were performed as described previously [6].

559 **Acknowledgements**

560 The authors thank Keith A. Laycock, PhD, ELS, for scientific editing of the manuscript. We thank
561 Dr. Richard Ashmun and the Flow Cytometry and Cell Sorting Shared Resource at St. Jude for
562 expert guidance, and the Childhood Solid Tumor Network (http://www.stjude.org/CSTN/) for
563 providing xenograft models. Preclinical imaging was performed with help from the Center for In
564 Vivo Therapeutics at St. Jude. Cell images were acquired at the Cell and Tissue Imaging Center,
565 cytogenetics were performed by the Cytogenetic Shared Resource, and microarray data were
566 generated at the Hartwell Center for Bioinformatics and Biotechnology, all of which are
567 supported by St. Jude and by the National Cancer Institute grant P30 CA021765. Additionally, this
568 work was supported by the American Lebanese Syrian Associated Charities (AS, E.A.S.). E.A.S.
569 was supported by the National Comprehensive Cancer Network and is a St. Baldrick's Scholar
570 with generous support from the Invictus Fund. A.A.S. was supported by the Sarcoma Foundation
571 of America and the St. Baldrick's Foundation. The content of this paper is solely the responsibility
572 of the authors and does not necessarily represent the official views of the National Institutes of
573 Health.

574

References

1. Pappo, A.S. and U. Dirksen, *Rhabdomyosarcoma, Ewing Sarcoma, and Other Round Cell Sarcomas.* J Clin Oncol, 2018. **36**(2): p. 168-179.
2. Womer, R.B., et al., *Randomized controlled trial of interval-compressed chemotherapy for the treatment of localized Ewing sarcoma: a report from the Children's Oncology Group.* J Clin Oncol, 2012. **30**(33): p. 4148-54.
3. Skapek, S.X., et al., *Rhabdomyosarcoma.* Nat Rev Dis Primers, 2019. **5**(1): p. 1.
4. Spunt, S.L., et al., *A risk-based treatment strategy for non-rhabdomyosarcoma soft-tissue sarcomas in patients younger than 30 years (ARST0332): a Children's Oncology Group prospective study.* Lancet Oncol, 2020. **21**(1): p. 145-161.
5. Kager, L., G. Tamamyan, and S. Bielack, *Novel insights and therapeutic interventions for pediatric osteosarcoma.* Future Oncol, 2017. **13**(4): p. 357-368.
6. Stewart, E., et al., *Targeting the DNA repair pathway in Ewing sarcoma.* Cell Rep, 2014. **9**(3): p. 829-41.
7. Federico, S., *A phase I trial of talazoparib and irinotecan with and without temozolomide in children and young adults with recurrent or refractory solid malignancies.* European Journal of Cancer, 2020. *In Press*.
8. Brenner, J.C., et al., *PARP-1 inhibition as a targeted strategy to treat Ewing's sarcoma.* Cancer Res, 2012. **72**(7): p. 1608-13.
9. Murai, J., et al., *Trapping of PARP1 and PARP2 by Clinical PARP Inhibitors.* Cancer Res, 2012. **72**(21): p. 5588-99.
10. Tang, S.W., et al., *SLFN11 Is a Transcriptional Target of EWS-FLI1 and a Determinant of Drug Response in Ewing Sarcoma.* Clin Cancer Res, 2015. **21**(18): p. 4184-93.
11. Gorthi, A., et al., *EWS-FLI1 increases transcription to cause R-loops and block BRCA1 repair in Ewing sarcoma.* Nature, 2018. **555**(7696): p. 387-391.
12. Choy, E., et al., *Phase II study of olaparib in patients with refractory Ewing sarcoma following failure of standard chemotherapy.* BMC Cancer, 2014. **14**: p. 813.
13. Ballestrero, A., et al., *Report on the first SLFN11 monothematic workshop: from function to role as a biomarker in cancer.* J Transl Med, 2017. **15**(1): p. 199.
14. Mu, Y., et al., *SLFN11 inhibits checkpoint maintenance and homologous recombination repair.* EMBO Rep, 2016. **17**(1): p. 94-109.
15. Murai, J., et al., *SLFN11 Blocks Stressed Replication Forks Independently of ATR.* Mol Cell, 2018. **69**(3): p. 371-384.e6.
16. Thomas, A. and Y. Pommier, *Targeting Topoisomerase I in the Era of Precision Medicine.* Clin Cancer Res, 2019. **25**(22): p. 6581-6589.
17. Murai, J., et al., *Rationale for poly(ADP-ribose) polymerase (PARP) inhibitors in combination therapy with camptothecins or temozolomide based on PARP trapping versus catalytic inhibition.* J Pharmacol Exp Ther, 2014. **349**(3): p. 408-16.
18. Zoppoli, G., et al., *Putative DNA/RNA helicase Schlafen-11 (SLFN11) sensitizes cancer cells to DNA-damaging agents.* Proc Natl Acad Sci U S A, 2012. **109**(37): p. 15030-5.
19. Coussy, F., et al., *BRCAness, SLFN11, and RB1 loss predict response to topoisomerase I inhibitors in triple-negative breast cancers.* Sci Transl Med, 2020. **12**(531).
20. Conteduca, V., et al., *SLFN11 Expression in Advanced Prostate Cancer and Response to Platinum-based Chemotherapy.* Mol Cancer Ther, 2020. **19**(5): p. 1157-1164.

21. Pietanza, M.C., et al., *Randomized, Double-Blind, Phase II Study of Temozolomide in Combination With Either Veliparib or Placebo in Patients With Relapsed-Sensitive or Refractory Small-Cell Lung Cancer.* J Clin Oncol, 2018. **36**(23): p. 2386-2394.
22. Gardner, E.E., et al., *Chemosensitive Relapse in Small Cell Lung Cancer Proceeds through an EZH2-SLFN11 Axis.* Cancer Cell, 2017. **31**(2): p. 286-299.
23. Garnett, M.J., et al., *Systematic identification of genomic markers of drug sensitivity in cancer cells.* Nature, 2012. **483**(7391): p. 570-5.
24. Maede, Y., et al., *Differential and common DNA repair pathways for topoisomerase I- and II-targeted drugs in a genetic DT40 repair cell screen panel.* Mol Cancer Ther, 2014. **13**(1): p. 214-20.
25. Bryant, H.E., et al., *Specific killing of BRCA2-deficient tumours with inhibitors of poly(ADP-ribose) polymerase.* Nature, 2005. **434**(7035): p. 913-7.
26. Keung, M.Y.T., Y. Wu, and J.V. Vadgama, *PARP Inhibitors as a Therapeutic Agent for Homologous Recombination Deficiency in Breast Cancers.* J Clin Med, 2019. **8**(4).
27. Davies, H., et al., *HRDetect is a predictor of BRCA1 and BRCA2 deficiency based on mutational signatures.* Nat Med, 2017. **23**(4): p. 517-525.
28. Kovac, M., et al., *Exome sequencing of osteosarcoma reveals mutation signatures reminiscent of BRCA deficiency.* Nat Commun, 2015. **6**: p. 8940.
29. Tirode, F., et al., *Genomic landscape of Ewing sarcoma defines an aggressive subtype with co-association of STAG2 and TP53 mutations.* Cancer Discov, 2014. **4**(11): p. 1342-53.
30. Crompton, B.D., et al., *The genomic landscape of pediatric Ewing sarcoma.* Cancer Discov, 2014. **4**(11): p. 1326-41.
31. Murai, J., et al., *Schlafen 11 (SLFN11), a restriction factor for replicative stress induced by DNA-targeting anti-cancer therapies.* Pharmacol Ther, 2019. **201**: p. 94-102.
32. Zhang, J., et al., *Targeting DNA Replication Stress for Cancer Therapy.* Genes (Basel), 2016. **7**(8).
33. Thomas, A. and Y. Pommier, *Targeting Topoisomerase I in the Era of Precision Medicine.* Clin Cancer Res, 2019.
34. Subramanian, A., et al., *Gene set enrichment analysis: a knowledge-based approach for interpreting genome-wide expression profiles.* Proc Natl Acad Sci U S A, 2005. **102**(43): p. 15545-50.
35. Krämer, A., et al., *Causal analysis approaches in Ingenuity Pathway Analysis.* Bioinformatics, 2014. **30**(4): p. 523-30.
36. Rabinovich, S., et al., *Diversion of aspartate in ASS1-deficient tumours fosters de novo pyrimidine synthesis.* Nature, 2015. **527**(7578): p. 379-383.
37. Keshet, R., et al., *Rewiring urea cycle metabolism in cancer to support anabolism.* Nat Rev Cancer, 2018. **18**(10): p. 634-645.
38. Bean, G.R., et al., *A metabolic synthetic lethal strategy with arginine deprivation and chloroquine leads to cell death in ASS1-deficient sarcomas.* Cell Death Dis, 2016. **7**(10): p. e2406.
39. Kremer, J.C., et al., *Arginine Deprivation Inhibits the Warburg Effect and Upregulates Glutamine Anaplerosis and Serine Biosynthesis in ASS1-Deficient Cancers.* Cell Rep, 2017. **18**(4): p. 991-1004.
40. May, W.A., et al., *Characterization and drug resistance patterns of Ewing's sarcoma family tumor cell lines.* PLoS One, 2013. **8**(12): p. e80060.
41. Heisey, D.A.R., et al., *The Ewing Family of Tumors Relies on BCL-2 and BCL-XL to Escape PARP Inhibitor Toxicity.* Clin Cancer Res, 2019. **25**(5): p. 1664-1675.
42. Schafer, E.S., et al., *Phase 1/2 trial of talazoparib in combination with temozolomide in children and adolescents with refractory/recurrent solid tumors including Ewing sarcoma: A Children's*

Oncology Group Phase 1 Consortium study (ADVL1411). Pediatr Blood Cancer, 2020. **67**(2): p. e28073.

	All, N=220 (%)	Survival Studies, N=143(%)
Age (years)		
N	185	135
Mean ± SD	9.2 ± 6.1	9.0 ± 6.4
Median (min - max)	9.6 (0.3 - 23.5)	8.8 (0.3 - 23.5)
Sex		
Female	82 (44.3)	63 (46.7)
Male	103 (55.7)	72 (53.3)
NA/missing	35	8
Race		
White	129 (74.1)	91 (71.7)
Black	34 (19.5)	26 (20.5)
Other	11 (6.3)	10 (7.9)
NA/missing	46	16
Ethnicity		
Non-Hispanic	123 (87.2)	97 (88.2)
Hispanic	18 (12.8)	13 (11.8)
NA/missing	79	33
Metastatic Disease		
No	68 (40.2)	43 (34.1)
Yes	101 (59.8)	83 (65.9)
NA/missing	51	17
Chemotherapy		
No	3 (1.7)	2 (1.6)
Yes	171 (98.3)	124 (98.4)
NA/missing	46	17
Radiation		
No	64 (36.8)	42 (33.3)
Yes	110 (63.2)	84 (66.7)
NA/missing	46	17
Surgery		
No	32 (18.4)	20 (15.9)
Yes	142 (81.6)	106 (84.1)
NA/missing	46	17
Transplantation		
No	127 (73.8)	84 (67.2)
Yes	45 (26.2)	41 (32.8)
NA/missing	48	18
Diagnosis Group		
DSRCT	7 (3.2)	5 (3.5)
aRMS	8 (3.6)	5 (3.5)
oRMS	1 (0.5)	5 (3.5)
eRMS	12 (5.5)	20 (14.0)
OS	55 (25.0)	42 (29.4)
NB	44 (20.0)	34 (23.8)
ES	48 (21.8)	13 (9.1)
NRSTS	19 (8.6)	19 (13.3)
sNOS	26 (11.8)	5 (3.5)

Table 1. Demographics of the pediatric cohort.

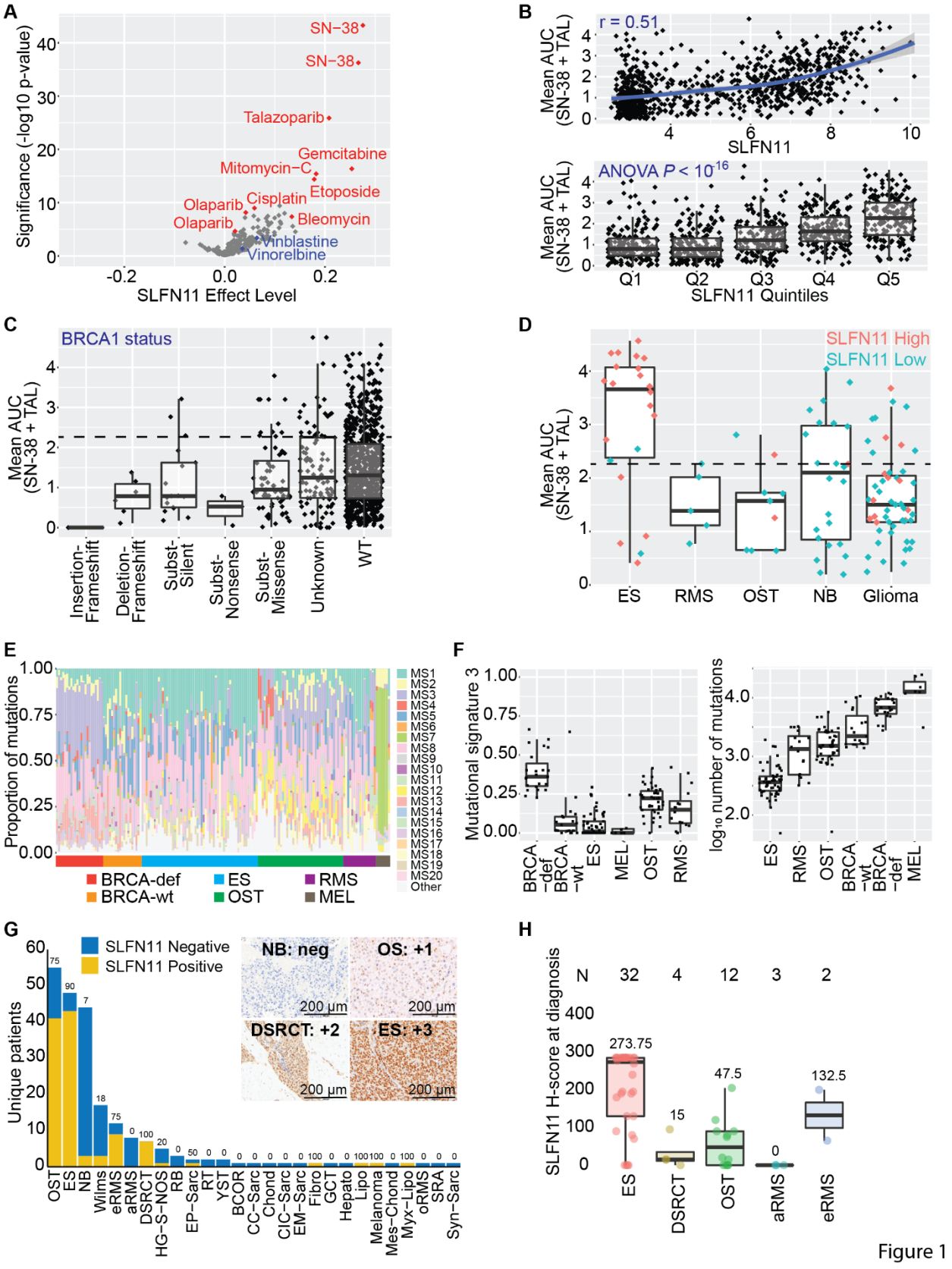

Figure 1

673 **Figure 1. SLFN11 was highly correlated with the efficacy of SN-38 and TAL, and was widely**
674 **expressed in pediatric sarcoma.** Correlation between SLFN11 expression and the single-agent
675 AUC **(A)** or mean **(B)** of the AUC for SN-38 and TAL after 72 h drug exposure as reported in the
676 GDSC database. Olaparib and SN-38 appeared as two different batches in the database. **(C)**
677 Correlation between the mean of the AUC for SN-38 and TAL from the GDSC and BRCA1
678 mutational status as annotated in the COSMIC database. Dotted line equals the median activity
679 of the highest quintile of SLFN11 expression ("Q5") from **(B)**. **(D)** Distribution of the mean of the
680 AUC for SN-38 and TAL from the GDSC in Ewing sarcoma (ES), rhabdomyosarcoma (RMS), OST
681 (osteosarcoma), NB (neuroblastoma), and glioma cell lines. Cells marked "SLFN11 High" (salmon)
682 expressed the highest quintile of SLFN11 expression ("Q5") from **(B),** while all others were
683 defined as "SLFN11 Low" (teal). Dotted line equals the median activity of the highest quintile of
684 SLFN11 expression ("Q5") from **(B)**. **(E-F)** Mutational signatures and total number of mutations
685 calculated from ES, RMS, and OST tumor samples from pediatric patients. BRCA-wt and BRCA-
686 deficient samples were included as controls for MS3. Melanoma was included as a positive
687 control for MS7. **(G)** SLFN11 status as assessed by immunohistochemistry in 353 samples from
688 220 unique patients treated on solid tumor protocols at our institution. "SLFN11 Negative" was
689 defined as H-score = 0, and "SLFN11 Positive" as H-score > 0. **(H)** SLFN11 H-score at diagnosis for
690 select pediatric sarcoma. The mean H-score is reported for each tumor type.
691

A

Tumor Model	Tumor Type	*EWSR1* Translocation	p53	SLFN11 Protein	TAL AUC 24	TAL AUC 48	TAL AUC 72	SN-38 AUC 24	SN-38 AUC 48	SN-38 AUC 72	Mean 72
ES8	ES	EWSR1-FLI1 type II	mut	1.00	0.26	0.40	0.49	0.39	0.54	0.65	0.57
A673-shEF	ES	EWSR1-FLI1 type I	mut	0.75	0.02	0.10	0.21	0.13	0.28	0.42	0.32
JN-DSRCT	DSRCT	EWSR1-WT1	wt	0.61	0.07	0.14	0.20	0.15	0.23	0.33	0.26
EW8	ES	EWSR1-FLI1 type I	mut	0.59	0.02	0.10	0.16	0.18	0.42	0.52	0.34
CADO-ES1	ES	EWSR1-ERG	wt	0.52	0.10	0.23	0.26	0.47	0.62	0.67	0.46
RH30	aRMS	NA	mut	0.49	0.00	0.12	0.09	0.37	0.59	0.44	0.27
ES1	ES	EWSR1-FLI1 type II	mut	0.47	0.16	0.31	0.47	0.35	0.54	0.60	0.53
H-EMC-SS	EMC	NA	wt	0.39	0.00	0.01	0.03	0.27	0.26	0.26	0.14
SAOS2	OST	NA	null	0.35	0.00	0.03	0.06	0.03	0.15	0.28	0.17
143B	OST	NA	mut	0.19	0.05	0.06	0.10	0.32	0.46	0.52	0.31
SJSA1	OST	NA	wt	0.06	0.00	0.01	0.02	0.11	0.09	0.10	0.06
RH3	aRMS	NA	mut	0.03	0.01	0.02	0.04	0.03	0.12	0.20	0.12
U2OS	OST	NA	wt	0.00	0.01	0.03	0.04	0.05	0.06	0.08	0.06
SU-CCS-1	CCS	EWSR1-ATF1	wt	0.00	0.00	0.01	0.05	0.09	0.16	0.23	0.14

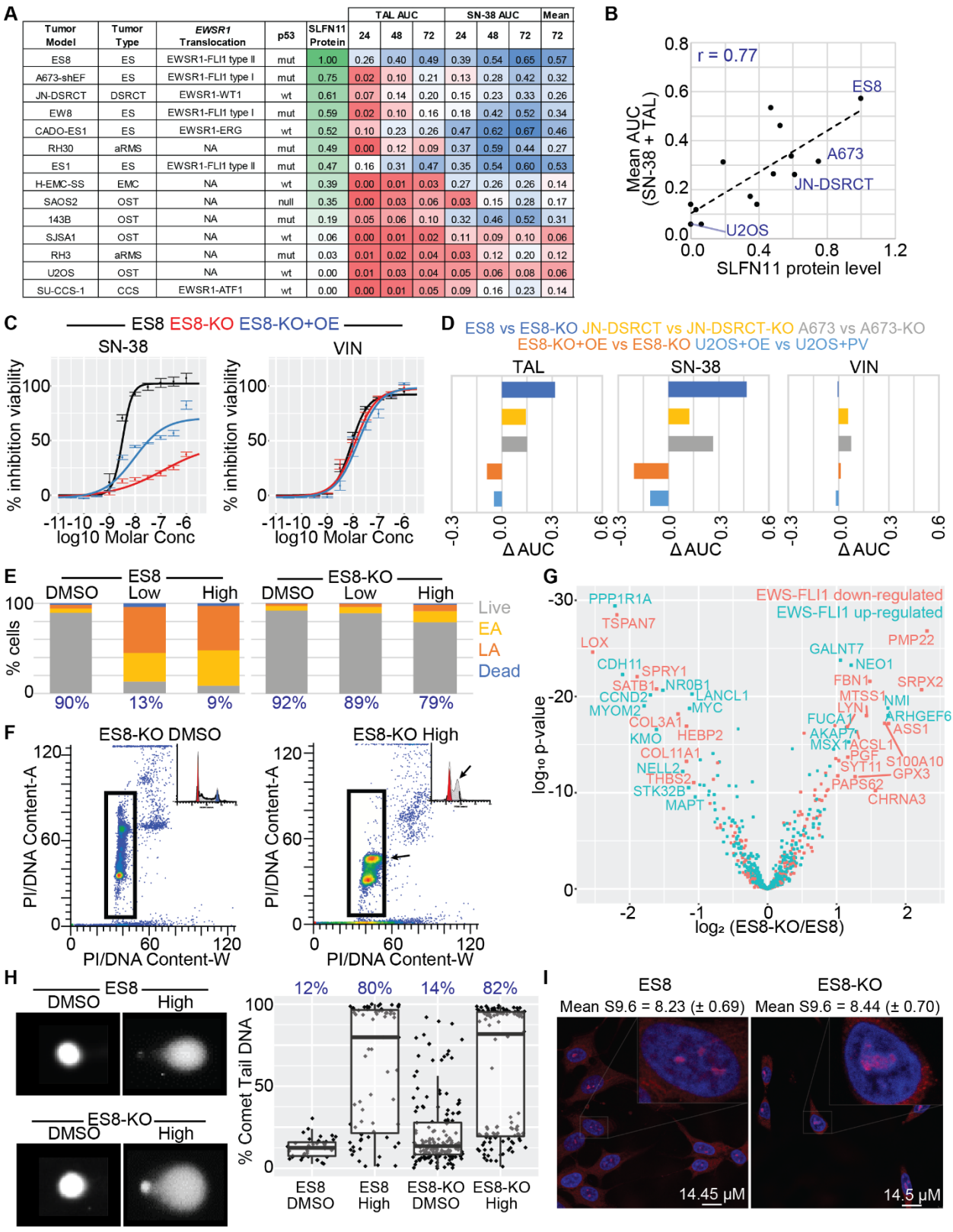

Figure 2

Figure 2. SLFN11, not *EWSR1*-translocation or R-loop expression, predicted sensitivity to SN-38 and TAL *in vitro*. (A) SLFN11 protein levels and CellTiter-Glo (CTG) results for 14 sarcoma cell lines that varied by translocation status, p53 status, and histology. Protein levels were normalized to ES8. The area-under-the-curve (AUC) for the dose-response curve was calculated at 24, 48, and 72 hours in the concentration range 10^{-11} to 10^{-4} Molar. Each value was then normalized to 700 – the maximum observed AUC for 100% efficacy at all concentrations in the range – yielding a number from 0 to 1. Although extraskeletal myxoid chondrosarcoma (EMC) cancers such as H-EMC-SS typically have *EWSR1-NR4A3* fusions, we did not detect a *EWSR1*-translocation in this line. $n \geq 2$. **(B)** Correlation between SLFN11 protein levels and the mean of the AUC for SN-38 and TAL for the cell panel in **(A)**. **(C)** CTG dose-response following 72h drug exposure of SN-38 and vincristine in ES8, ES8-KO, and ES8-KO+OE cells. $n \geq 2$. **(D)** Difference in normalized CTG AUC following 72 h drug exposure of TAL, SN-38, and vincristine in knockout and over-expression models. $n \geq 2$. **(E)** Flow cytometry assessment of cytotoxicity in ES8 and ES8-KO cells following 24h exposure to 'Low' (10 nM SN-38 + 10 nM TAL) and 'High' (1 µM SN-38 and 1 µM TAL) drug combinations. The percent live cells is reported in blue. EA = early apoptosis. LA = late apoptosis. $n \geq 2$. **(F)** Cell cycle analysis of ES8-KO cells following 24 h exposure to 'Low' SN-38+TAL. Arrows highlight the build-up of S-phase cells induced by the drug combination. **(G)** Volcano plot showing the difference in expression of reported EWS-FLI1 downregulated (salmon) and upregulated (teal) genes between ES8 and ES8-KO cells. Expression was assessed by microarray at 4 h and 24 h following exposure to 0 and 2 Gy. $n = 3$. **(H)** Exemplar image and quantification of the alkaline comet tail assay of ES8 and ES8-KO cells following 2.5h exposure to the 'High' concentration of SN-38 and TAL. Mean percent comet tail DNA is reported in blue. **(I)** Immunofluorescence

715 quantification of R-loops in untreated ES8 and ES8-KO cells. Nuclei were stained with DAPI (blue)

716 and R-loops were stained with S9.6 antibody (red). Mean (sem) S9.6 nuclear intensity is reported.

717

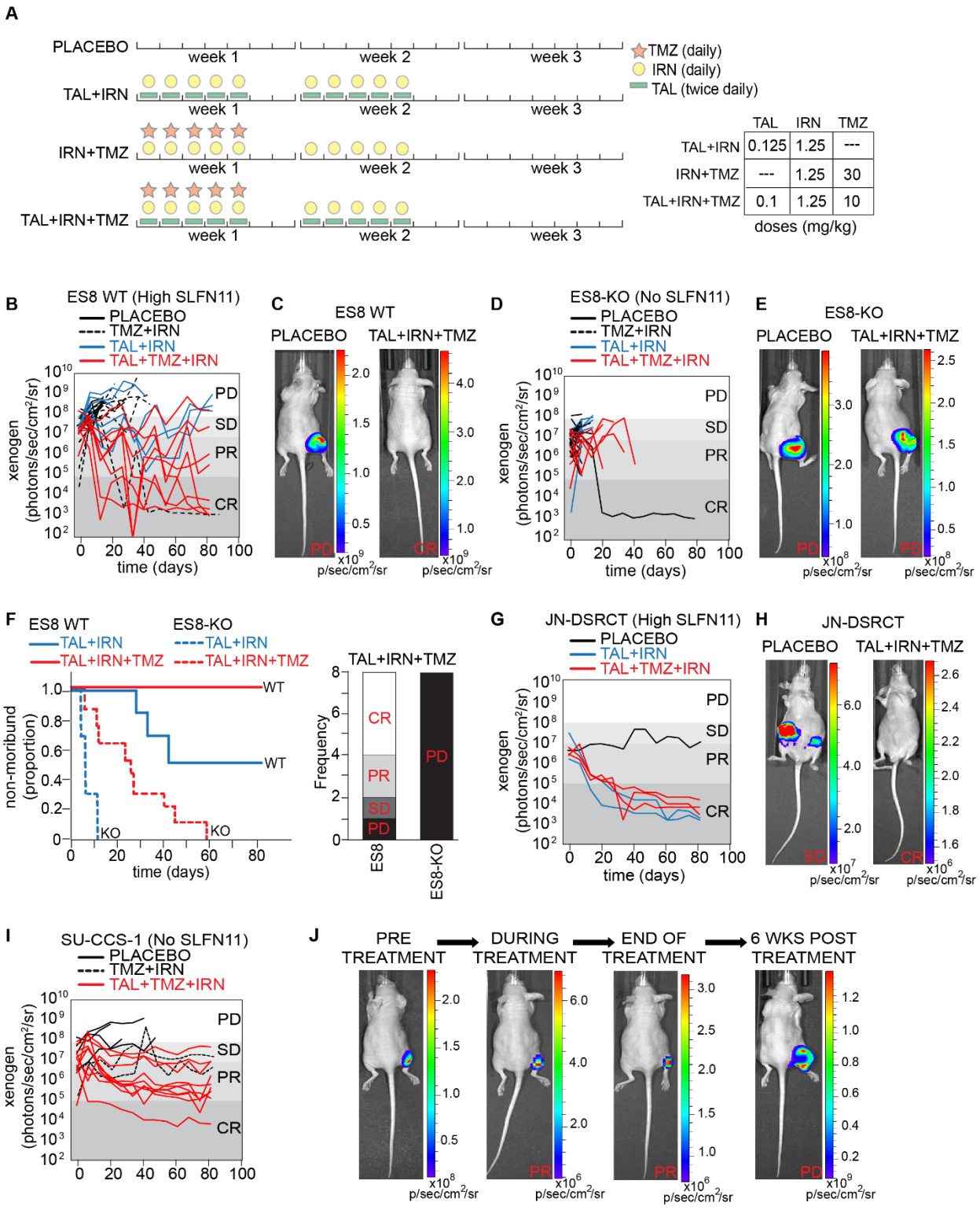

Figure 3

720 **Figure 3. SLFN11, not *EWSR1*-translocation, was required for sensitivity to SN-38 and TAL *in**

721 ***vivo.* (A)** Drug schedule selected for each combination treatment regimen. **(B)** Line plot of tumor

722 burden over time as measured by bioluminescence for ES8 xenografts. Each line is a different

723 mouse. **(C)** Representative images from the study in **(B)** are shown with PD in the placebo control

724 group and a CR in the TAL+TMZ+IRN group. **(D)** Line plot of tumor burden over time for ES8-KO

725 xenografts. **(E)** Representative images from the study in **(D)** are shown with PD in both the

726 placebo and TAL+TMZ+IRN groups. **(F)** Survival curves and response at end of treatment with

727 TAL+TMZ+IRN for ES8 and ES8-KO models. **(G)** Line plot of tumor burden over time for JN-DSRCT

728 xenografts. **(H)** Representative images from the study in **(G)** are shown with PD in the placebo

729 group and a CR in the TAL+TMZ+IRN group. **(I)** Line plot of tumor burden over time for SU-CCS-1

730 xenografts. **(J)** Representative images of a mouse treated over time in the TAL+TMZ+IRN group

731 from **(I)** showing a PR during treatment and regrowth of tumor upon stopping therapy. PD,

732 progressive disease; SD, stable disease; PR, partial response; CR, complete response.

733

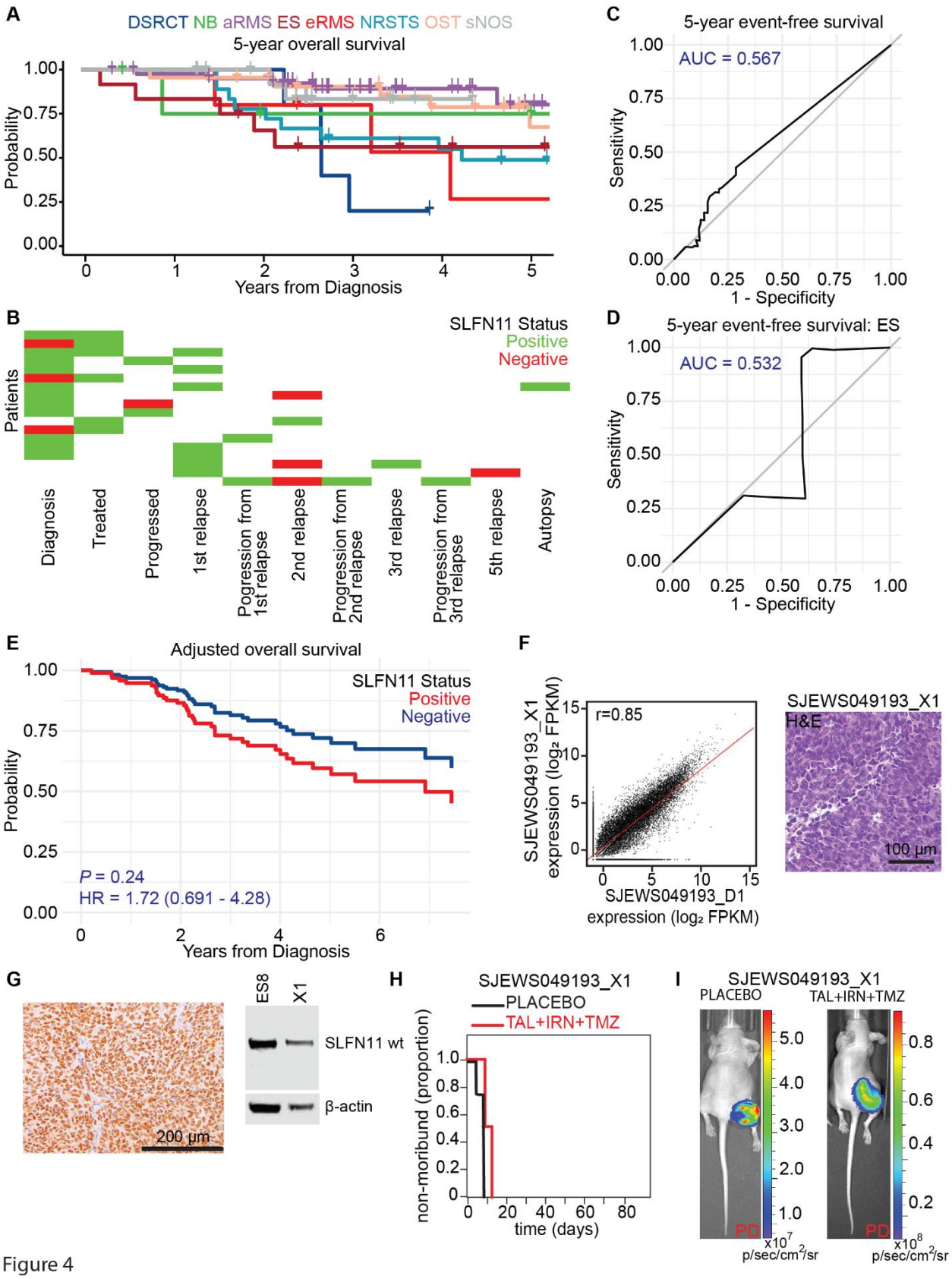

 Figure 4

735 **Figure 4. SLFN11 expression was not associated with better outcomes in children with**
736 **sarcomas. (A)** Five-year overall survival rates by diagnosis for the sarcoma patients in our IHC
737 study. **(B)** SLFN11 status for 18 patients with at least two SLFN11 IHC measurements spanning
738 different points in treatment. “Negative” and “Positive” SLFN11 status were defined as H-score
739 equal to zero and H-score greater than 0, respectively. **(C)** ROC curve for five-year event free
740 survival of all sarcoma patients as a function of H-score. **(D)** ROC curve for five-year event free
741 survival of ES patients as a function of H-score**. (E)** Adjusted overall survival as a function of
742 SLFN11 status after controlling for age, metastatic status, and disease. **(F)** RNA-seq expression
743 profile comparing the ES patient-derived orthotopic xenograft model SJEWS049193_X1 and the
744 matched primary tumor (SJEWS049193_D1, Pearson r = 0.85), and hematoxylin and eosin stain
745 of SJEWS049193_X1. **(G)** SLFN11 IHC and Western blot from a SJEWS049193_X1 tumor sample.
746 **(H)** Survival curves for SJEWS049193_X1 and **(I)** representative images from the efficacy study
747 showing progressive disease (PD) in both the placebo and TAL+TMZ+IRN groups.
748

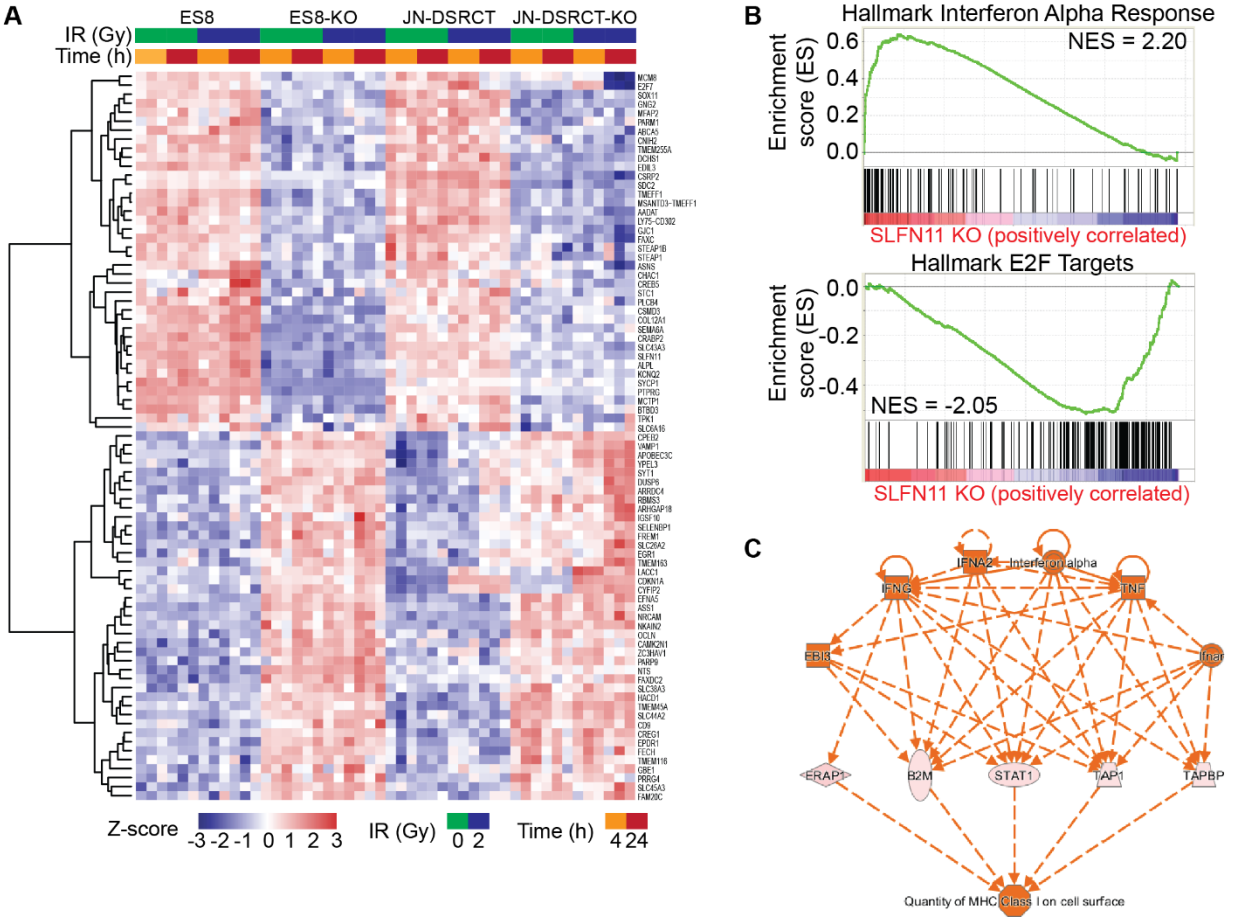

D

Gene Symbol	ES8 KO vs WT	JN-DSRCT KO vs WT	Mean KO vs WT
ASS1	1.76	1.66	1.71
TMEM45A	1.01	2.15	1.58
NTS	2.45	0.59	1.52
APOBEC3C	0.98	1.84	1.41
FAXDC2	2.05	0.56	1.30
GRB14	-2.43	-0.43	-1.43
CRABP2	-2.70	-0.86	-1.78
SLC43A3	-2.37	-1.41	-1.89
PTPRG	-3.38	-0.89	-2.13
SYCP1	-4.58	-0.53	-2.55

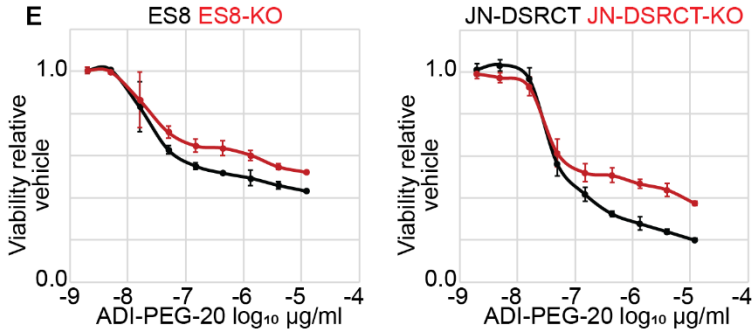

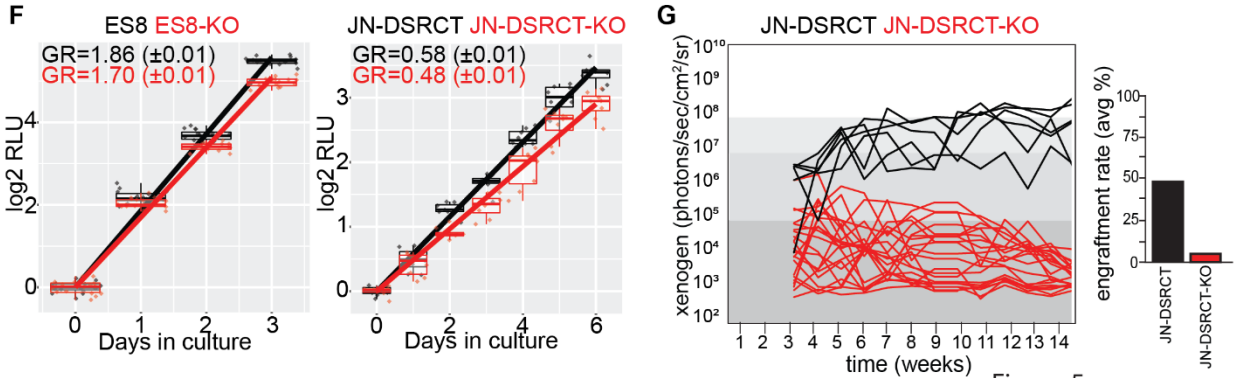

Figure 5

Figure 5. SLFN11 augmented metabolism, evasion from the innate immune response, and proliferation in pediatric sarcomas. (A) Heatmap of the most consistently differentially expressed genes (≥0.5 $\log_2$ unit change in the same direction) from a microarray experiment comparing ES8 and JN-DSRCT WT and KO cell lines at 4 h and 24 h following exposure to 0 and 2 Gy. n = 3. **(B)** Highest scoring GSEA Hallmark gene sets enriched in KO (top) and wild-type (bottom) lines. **(C)** The top regulator in KO cells identified via IPA upstream regulator analysis. **(D)** Top five most differentially activated or inhibited genes ($\log_2$ change in expression) in KO vs wild-type cells. **(E)** CTG assay assessing viability in KO and wild-type cells exposed to the pegylated arginine deiminase ADI-PEG-20. **(F)** Growth rate (GR) determination in KO vs wild-type cells, expressed as doublings/day (sem). **(G)** *In vivo* growth rate assessment comparing JN-DSRCT wild-type and KO models. Each cell line was injected at a cell density of 1 million cells/mouse. Xenogen measurements were started after 3-4 weeks for JN-DSRCT or JN-DSRCT-KO, then continued weekly.

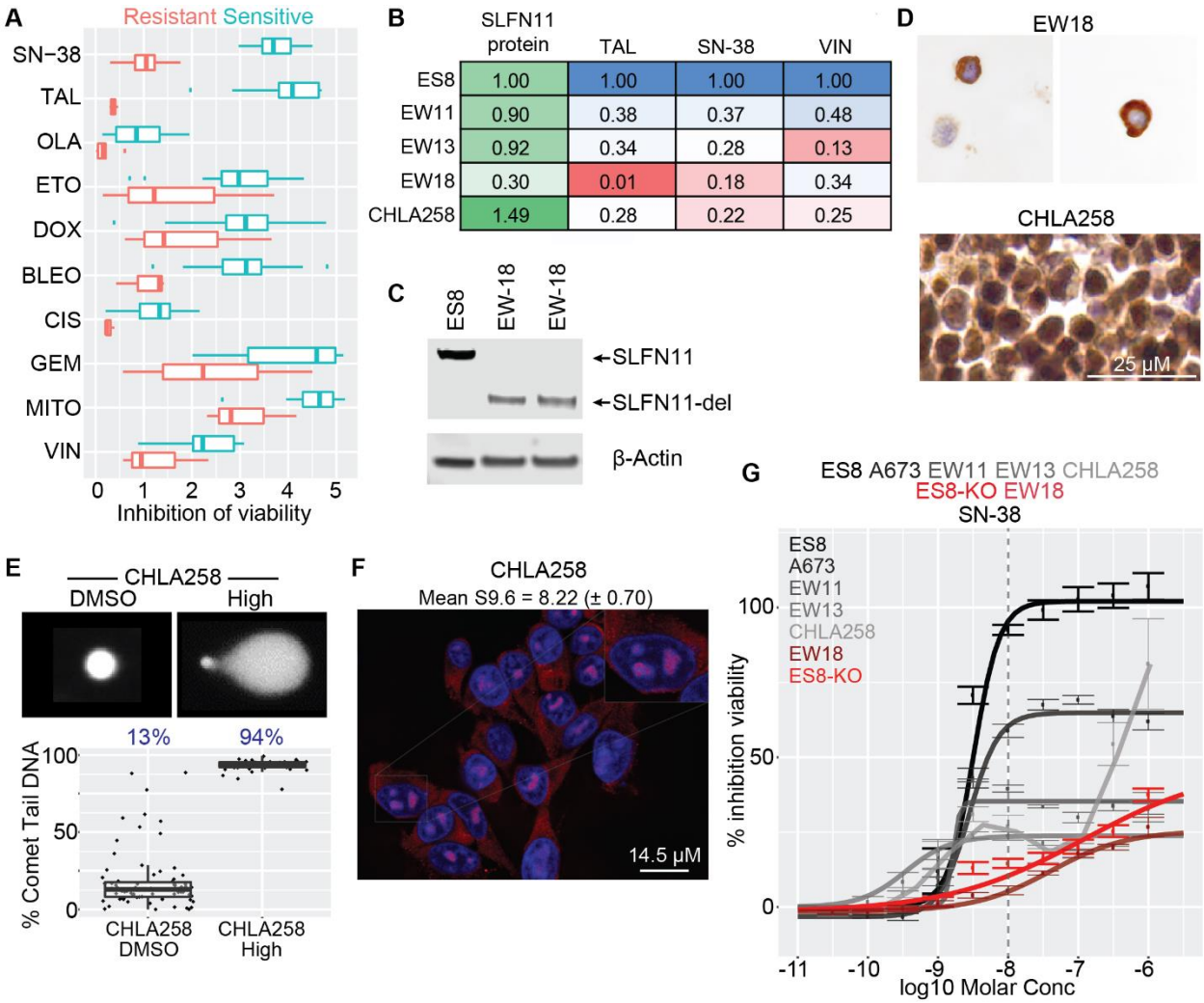

Figure 6

765 **Figure 6. BCL-Xli restored sensitivity to SN-38 and TAL in resistant SLFN11 expressing sarcoma**
766 **cells. (A)** Boxplot comparing drug sensitivity in resistant and sensitive ES cell lines from the GDSC.
767 **(B)** Heatmap of AUC values in four resistant ES cell lines normalized to ES8 (CTG assay, 72h drug
768 exposure). n ≥ 2. **(C)** Western blot from two biological replicates of EW-18 confirming expression
769 of a truncated SLFN11 protein. **(D)** Confirmation of cytoplasmic and nuclear staining of SLFN11 in
770 EW-18 and CHLA258, respectively. **(E)** Exemplar image and quantification of the alkaline comet
771 tail assay of CHLA258 cells following 2.5 h exposure to the "High" concentration of SN-38 and
772 TAL. Mean percent comet tail DNA is reported in blue. **(F)** Immunofluorescence quantification of
773 R-loops in untreated CHLA258 cells. Nuclei were stained with DAPI (blue) and R-loops were
774 stained with S9.6 antibody (red). Mean (sem) S9.6 nuclear intensity is reported. **(G)** Dose-
775 response curves for SN-38 (CTG, 72 h) in ES8 (black), SLFN11 expressing resistant ES cell lines
776 (grays), ES8 KO (red), and EW-18 (dark red). n ≥ 2. **(H)** Dose-response curves for SN-38 and TAL
777 (CTG, 72 h) in ES8 (black), ES8-KO (red), 2 ES8 BAK KO models (blue), 2 ES8 BAX KO models (green),
778 and 2 ES8 BAK-KAX double KO models (purple). n ≥ 2. **(I)** Heatmap of AUC values in ES8-KO and
779 the BAK, BAX, and BAK-BAX KO models normalized to ES8 (CTG assay, 72 h drug exposure). n ≥ 2.
780 **(J)** Dose-response curves for a 1:1 mixture of SN-38 and TAL combined with either vehicle (DMSO,
781 black), 1 μM venetoclax ("BCL2i", green), 1 μM S63845 ("MCL1i", blue), or 1 μM A-1331852 ("BCL-
782 Xli", red) (CTG, 72 h). n ≥ 2.